Insights into Airframe Aerodynamics and Rotor-on-Wing Interactions from a 0.25-Scale Tiltrotor Wind Tunnel Model

L.A. Young
D. Lillie
M. McCluer
G.K. Yamauchi

Army/NASA Rotorcraft Division
NASA Ames Research Center
Moffett Field, CA 94035

M.R. Derby
Aerospace Computing, Inc.
Mountain View, CA

Abstract

A recent experimental investigation into tiltrotor aerodynamics and acoustics has resulted in the acquisition of a set of data related to tiltrotor airframe aerodynamics and rotor and wing interactional aerodynamics. This work was conducted in the National Full-scale Aerodynamics Complex's (NFAC) 40-by-80 Foot Wind Tunnel, at NASA Ames Research Center, on the Full-Span Tilt Rotor Aeroacoustic Model (TRAM). The full-span TRAM wind tunnel test stand is nominally based on a quarter-scale representation of the V-22 aircraft. The data acquired will enable the refinement of analytical tools for the prediction of tiltrotor aeromechanics and aeroacoustics.

Nomenclature

c	Wing reference chord length, 2.0833 ft
C_D	Airframe drag coefficient
C_L	Airframe (including wing) lift coefficient
C_N	Wing section normal force coefficient
C_P	Rotor power coefficient
C_T	Rotor thrust coefficient
DL	Hover download, lb
FM	Rotor hover figure of merit
i_N	Nacelle incidence angle, deg.
M_{Tip}	Rotor tip Mach number
p_u, p_ℓ	Wing upper and lower wing static pressures, psig
r/R	'Radial' (measured from rotor hub) spanwise location of wing static pressure taps
R	Rotor radius, 4.75 ft
S	Wing reference area, 23.9 ft^2
T	Rotor Thrust, lb
V	Wind tunnel test section velocity, fps
x/c	Wing static pressure tap chordwise location
α_F	Fuselage angle of attack, deg.
α_s	Rotor shaft angle, deg, shaft vertical at zero degrees angle, positive aft
δ_f	Flaperon angles, deg.
δ_e	Elevator angle, deg.
μ	Advance ratio, $V/\Omega R$
Ω	Rotor rotational speed, radians/sec

Introduction

The development of the Tilt Rotor Aeroacoustic Model (TRAM) has been a joint effort of NASA Ames and Langley Research Centers and the U.S. Army Aeroflightdynamics Directorate (AFDD). Wind tunnel test results were acquired in support of the NASA Short Haul Civil Tiltrotor (SHCT) and Rotorcraft R&T Base programs. Two wind tunnel test campaigns have

been conducted to date with the TRAM test stand: an isolated rotor test in the Duits-Nederlandse Windtunnel (DNW) in December 1997 and April-May 1998; a full-span, dual-rotor, complete-airframe wind tunnel model test in NASA Ames' National Full-scale Complex (NFAC) 40-by-80 Foot Wind Tunnel in November-December 2000. In addition to acquiring fundamental aeromechanics and aeroacoustic data during these tests, wing static pressure measurements were made characterizing tiltrotor airframe aerodynamics and rotor-on-wing interactional aerodynamics.

This paper discusses the wing pressures and model balance measurements acquired with and without the rotors installed on the full-span TRAM. Results from several different model configurations and test conditions are presented.

Description of TRAM Test Stand

TRAM can be configured as either an isolated rotor test stand or a full-span, dual rotor aircraft model. Figures 1 and 2 show the isolated rotor and full-span TRAM configurations, respectively. The rotors and test model are nominally a quarter-scale representation of the V-22 Osprey tiltrotor aircraft (Refs. 1-3).

Fig. 1 -- Isolated rotor TRAM configuration (Installed in DNW Open-Jet Test Section)

Fig. 2 -- Full-span TRAM configuration (Prior to NFAC Tunnel Entry)

The ability to configure the TRAM test stand as either an isolated rotor or dual-rotor full-span aircraft model makes it uniquely suited for identifying and studying tiltrotor aerodynamics and acoustics in a rigorous experimental manner. The drive train, nacelle assembly, hub and rotor components from the isolated rotor model are also used to make up the right-hand rotor and nacelle assembly on the full-span model. Each rotor is powered by an electric motor designed to deliver up to 300 hp at 1588 rpm (through an 11.3:1 gear reduction in the model drive train). An interconnect shaft insures that both rotors can be driven by one motor, if necessary.

The right-hand rotor has a set of pressure-instrumented blades and a set of strain-gauged blades; the left-hand rotor blades have only strain gauge instrumentation. Only the strain-gaged blades were tested in the 40-by-80 Foot Wind Tunnel test. A rotating amplifier system was used to condition signals from the heavily instrumented right-hand rotor. The TRAM blades and hub retention system are fabricated with composite materials and are structurally tailored to match fundamental frequencies of the full-scale aircraft. The hub and control system are kinematically similar to the full-scale aircraft. Both left-hand and right-hand rotor forces and moments are measured with strain-gauged balances located in each pylon assembly. The overall aerodynamic loads on the full-span model are measured with a strain-gauged balance located in the fuselage. A more detailed description of the TRAM test stands can be found in Refs. 1-2. A more comprehensive discussion of the full-span TRAM 40-by-80 Foot Wind Tunnel test can be found in Ref. 4.

Left-Hand-Wing and Flap Static Pressure Measurements

Wing pressure measurements were acquired from 185 static pressure taps installed on the left-hand wing and flaperons of the Full-Span TRAM. These measurements are used to study wing lift and normal forces in hover, helicopter mode, and airplane mode test conditions.

The wing static pressure tap locations, the expected pressure range, and the maximum expected dynamic pressure were defined, in part, based on results and insights from previous tiltrotor semispan wing testing (Ref. 5-6). An electronic pressure scanning system, made by PSI, was used to acquire data. The 185 taps are divided amongst 4 modules, each with a range of ±2.5 psid. Table 1 lists the locations of each module.

Table 1 -- PSI Module Locations on Left Wing

Module Description	Location
48-port, 90 deg tube	Cove/spar cap
48-port, 90 deg tube	Outboard flap
64-port, 90 deg tube	Inboard flap
64-port, 90 deg tube	Wing leading edge

The left wing's spanwise pressure stations are shown in Fig. 3. Pressure taps are located along the span of the left wing and are identified as a function of the left rotor radius, r/R (origin at the LH rotor shaft axis). Keeping in mind that the left rotor turns clockwise when viewed from above, the definitions for the r/R station are determined when the retreating blade is parallel with the wing's forward swept leading edge. Spanwise (r/R) wing pressure stations are parallel with tunnel flow, and not wing chord. Note that fuselage taps were not installed for the full-span TRAM testing. Fig. 4 shows a wing cross section at on spanwise station.
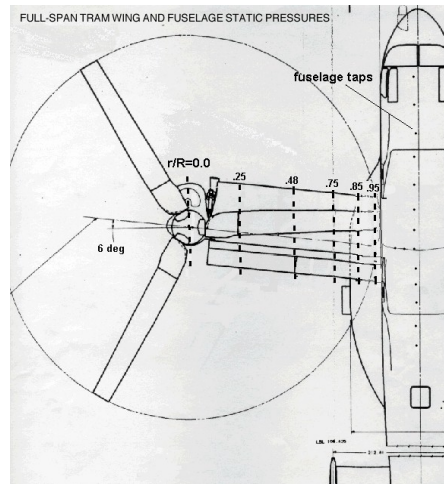

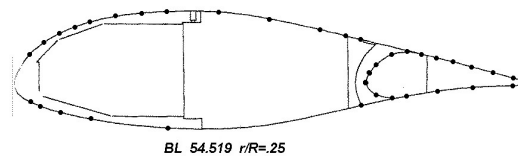Fig. 3 – Planform View of TRAM Wing and Spanwise Location of Static Pressure Taps

Fig. 4 – Chordwise Wing Pressure Taps (One Spanwise Station)

Table 2 summarizes the x/c chordwise locations for the wing pressure taps for the five spanwise wing r/R stations.

Table 2 – Left Hand Wing Pressure Tap Locations

	0.25 r/R	0.48	0.75	0.85	0.972
Upper Wing	.03,.06,.09, .12,.15,.2, .25,.3,.4,.5, .6,.65,.68	.03,.06,.09, .12,.15,.2, .25,.3,.4,.5, .588,.65, .68	.03,.06,.09, .12,.15,.2, .254,.3,.4, .5,.6,.65, .68	.03,.06,.09, .12,.15,.2, .25,.3,.4,.5, .6,.65,.68	.03,.06,.09, .12,.15,.2, .25,.3,.4,.5, .6,.65,.68
Upper Flap.	.686,.696, .71,.74,.77, .8,.83,.86, .9,.94,.98	.686,.696, .71,.74,.77, .8,.83,.86, .9,.94,.98	.686,.696, .71,.74,.77, .8,.83,.86, .9,.94,.98	.686,.696, .71,.74,.77, .8,.83,.86, .9,.94,.98	.686,.696, .71,.74,.77, .8,.83,.86, .9,.94,.98
Lower Wing	.001,.03, .05,.09,.15, .3,.68	.001,.03, .05,.09,.15, .25,.68	.001,.03, .05,.09,.2, .6,.68	.001,.03, .05,.09,.12, .15,.68	.001,.03, .05,.09,.12, .15,.68
Lower Flap.	.71,.74,.77, .83,.9,.98	.71,.74,.77, .83,.9,.98	.71,.74,.77, .83,.9,.98	.71,.74,.77, .83,.9,.98	.71,.74,.77, .83,.9,.98

Heater boxes were not be used with the PSI modules during the full-span TRAM test. Since

data drift caused by thermal effects was anticipated, a frequent calibration of the PSI system was performed. The PSI system was calibrated by taking 1024 samples at 10 different pressure settings (ranging from ±2.5 psid). The calibration and test data were low-pass filtered at ~4Hz using 1024 point FFT. The calibration coefficients were computed using a 2nd order least squares fit on the averages from each pressure setting. The reference pressure for the modules was the tunnel barometric pressure. The last port of each module measured the tunnel barometric pressure. Hence, the last port of each module provided an indication of the amount of signal drift during a test run, since, ideally, this port should provide a zero reading with zero drift. The results from each calibration were written to a computer file. Raw pressure data and reduced engineering unit measurements were saved to computer files for each data point.

Experimental Results

This paper discusses three categories of experimental observations from the full-span TRAM 40-by-80 Foot Wind Tunnel test. First, rotor and wing interactions in hover will be discussed, with emphasis on wing download. Second, rotor-on-wing interactions in helicopter-mode forward-flight will be discussed, presenting rotor and model loads and wing pressure distributions for rotor-on and rotor-off test points. Finally, balance loads and wing pressures (airframe only, no rotors) in airplane-mode forward-flight will be presented.

Rotor and Wing Interactions in Hover

Figure 5 shows the installation of the full-span TRAM test stand in the National Full-scale Aerodynamics Complex (NFAC) 40-by-80 Foot Wind Tunnel. One of the key concerns underlying any wind tunnel investigation is the impact of the tunnel test section on the test model (and rotor) aerodynamics and performance, and the determination of installation configurations and/or tunnel correction methodologies that minimize that influence. This is a particularly crucial issue for hover performance measurements in an enclosed wind tunnel environment. Wall effects, including flow recirculation, can be considerable if the rotor diameter is too large, or the disk loading too high, for the test section size.

Fig. 5 – Full-Span TRAM Installation in the NFAC 40-by-80 Foot Wind Tunnel

The NFAC 40-by-80 foot test section is an elliptical test section that has ceiling 'clam shell' doors that open up to expedite the installation of test models using an overhead high-capacity crane. The TRAM rotor hubs – at a fuselage angle of attack of zero degrees – are 21.8 feet above the tunnel floor, when the model is in helicopter-mode (i_N = 90 deg.). To minimize adverse wall effects on the full-span TRAM rotor hover performance measurements, the tunnel ceiling clam shells were left fully open, the model was pitched nose down to a fuselage angle of attack of –9 deg., and the tunnel (downstream) air exchangers were open to 50%. Figure 6 shows for a relatively low thrust coefficient of 0.0043 that that there is minimal observed influence, or variation, of the wind tunnel wall effects on rotor performance for the full-span TRAM installation (as represented by the minimum variation in the rotor power coefficient). As can also be seen in Fig. 6, there may be a slight 'ground effect' due to the rotor wake interaction with the tunnel floor (manifesting as a slightly reduced power level). Sweeping the fuselage angle of attack to -9 deg. appears to yield slightly high power levels.
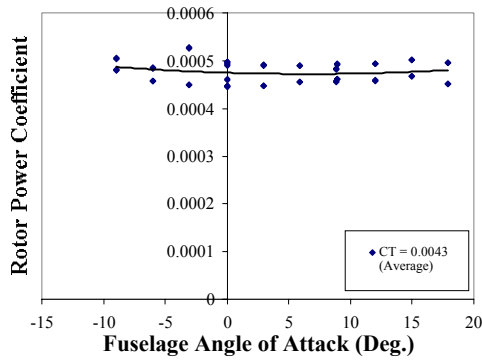
Fig. 6 – Influence of Wind Tunnel Test Section
Interactions in Hover

Fig. 7 – Influence of Wing/Airframe on Rotor
Hover Performance

Figure 7 compares the hover figure of merit performance data from the full-span TRAM test (i_N=90 deg. and α_F=-9 deg.) against isolated rotor TRAM data from the DNW (airplane-mode configuration). Both primary and secondary, left and right, rotor balance loads are included in the full-span figure of merit data. The blade, rotor, and nacelle assembly designs used for the isolated rotor and full-span TRAM tests are identical; in many cases the same hardware was used for the two tests (the full-span TRAM right-hand hub and nacelle assembly were used in the DNW isolated rotor test). Figure 7 shows a significant interactional (rotor-on-rotor and wing-on-rotor) aerodynamic effect in the full-span performance data. This result is preliminary but suggests that further investigation of interactional aerodynamic phenomena for tiltrotor hover performance is warranted. Though interactional aerodynamic investigations have been performed for tiltrotor aircraft previously (notably, Ref. 7), TRAM testing represents an opportunity to systematically explore these phenomena using a versatile modular test stand. It is anticipated – as has already begun with the isolated rotor TRAM data (Ref. 8) – that full-span TRAM data will enable the development/refinement of comprehensive design and analysis tools for tiltrotor aircraft.
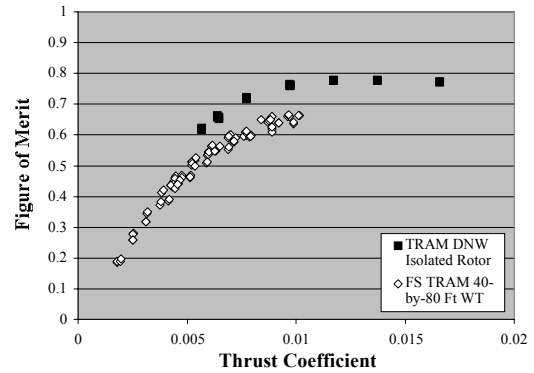
Two representative chordwise static pressure distribution plots are shown in Fig. 8, for spanwise locations 0.25 and 0.85 r/R. The chordwise location, x/c, is given in terms of the static pressure taps 'undeflected' (with respect to flaperon angle) positions. The rotor tip Mach number is 0.629, the left-hand rotor thrust is 378 lb (C_T = 0.0046), the nacelle incidence angle is 90 degrees, and the flaperon angles are uniformly set at 70 degrees.

(a)

(b)
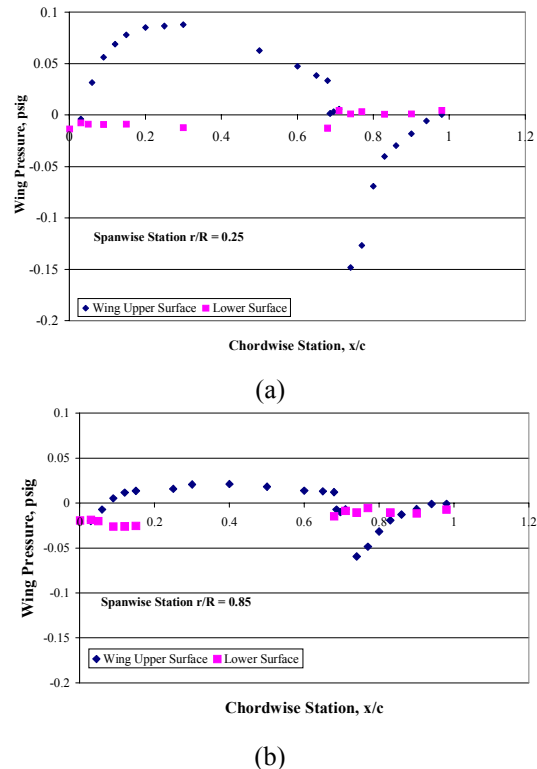
Fig. 8a-b– Sample of Wing Chordwise Pressure
Distributions (C_T = 0.0046)

Flaperon cove seals are implemented on the wing by thin, pre-loaded, fiberglass strips. Ideally, no flow (from lower to upper surface) should occur as a consequence of the fiberglass cove seals. The flaperons were remotely controlled in two discrete angle ranges: –10 to +35 deg. (positive trailing edge down) for airplane-mode operation and +35 to +100 degrees for hover and helicopter-mode forward flight. The flaperons' mechanical linkages must be manually adjusted to switch between the two discrete operating ranges. For each set of flaperons on the left and right side of the wing there was a pair of inboard and outboard flaps. Though each flaperon (of the four total) can be remotely controlled, all flaperons were set at the same angle for all test conditions. A separate set of fiberglass cove seals was used for the two different flaperon ranges.

A large amount of hover wing pressure data was acquired during the full-span TRAM test. This included data at several different rotor thrust conditions, flaperon angles, and nacelle incidence angles. Wing pressure data can be integrated (from $r/R = 0$, at the wing tip, to $r/R=1.21$, at the fuselage plane of symmetry) to provide estimates of the wing sectional normal force (i.e. download for hover test conditions), as shown in Fig. 9. Figure 9 is derived from the same test point and wing pressure data set that Fig. 8a-b are samples plots of.
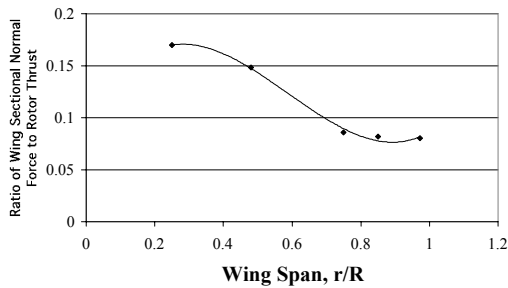

Fig. 9 – Representative Wing Integrated Sectional Download Results (C_T=0.0046)

Spanwise integration (applying the wing symmetry condition) of the Fig. 9 results yields an estimate for the TRAM download-to-thrust ratio of DL/T=0.105 for this test condition. This estimate of download-to-thrust ratio is typical of results previously noted in the literature (Refs. 5-7, 9).

Both chordwise and spanwise integration of the wing pressure data was accomplished by simple trapezoidal rule numerical integration. The integration limit values for the leading and trailing edge of the flaperons were assumed to be the mean value of the nearest adjacent upper and lower surface pressure tap measurements, for chordwise integration. A leading edge pressure tap was provided for the main wing section. For spanwise integration, the sectional normal force loading at the wing tip ($r/R=0$) was assumed to be zero and to be constant/uniform loading from the last measurement station, $r/R=0.972$, to $r/R=1.21$ (fuselage plane of symmetry). Symmetry (left- versus right-hand wing) was also assumed.

Figure 10 is a qualitative comparison of hover download results between two tiltrotor tests/configurations. Hover download estimates from the 0.25-scale full-span TRAM integrated wing pressures are (i_N = 90 deg., M_{Tip} = 0.63, and δ_f= 70 deg.) compared to results from a 0.658-scale JVX proprotor, semispan wing, and image plane, Ref. 5 (i_N = 85 deg., M_{Tip} = 0.71, and δ_f= 67 deg.). Two observations readily stand out from this qualitative comparison. First, despite the nontrivial model configuration and operating condition differences between the two tests, the download results appear to be in good agreement with each other for thrust coefficients greater than 0.005. Second, the download-to-thrust ratio trend, though seemingly linear and/or asymptotic at thrust coefficients representative of the nominal operating conditions for conventional tiltrotor aircraft, appears to steeply rise for very low thrust coefficients.
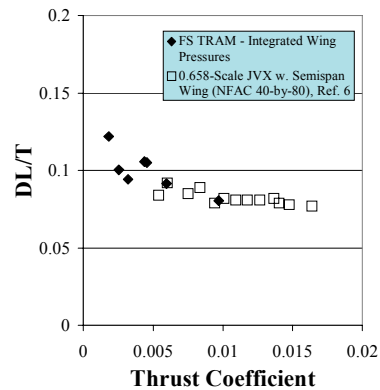

Fig. 10 – Qualitative Data Comparison Between Tiltrotor Hover Download Tests/Configurations

Figure 11 is a comparison of the full-span TRAM hover download test results derived from integrated wing pressures versus the measured download from the model balances. The download-to-thrust ratio from the model balances was derived as $DL/T = 1 - T_F/(T_R + T_L)$, for hover testing at nacelle incidence angles of ninety degrees. T_R and T_L are rotor thrust measurements from the right and left rotor balances, and T_F is the resolved model 'thrust' measurement from the fuselage balance, which measures the total model loads – including rotor loads. Figure 11 also demonstrates that the download contributions of the fuselage – in addition to the wing download component – is a significant fraction of an overall 'airframe' (wing and fuselage) hover download. This result is consistent with the experimental observations of Ref. 10 which estimated the fuselage contribution to total download to be between 36 to 42%. Still, there is considerable data scatter in the fuselage balance download results and additional testing in the future will be required to fully characterize the fuselage contribution to aircraft download.
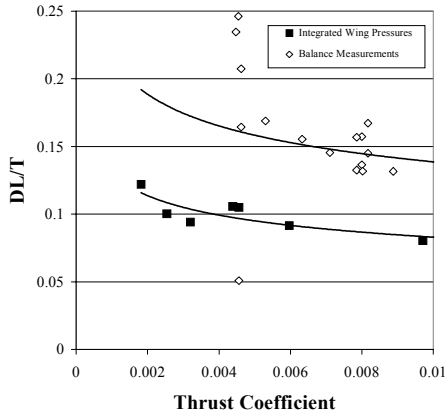
Fig. 11 – Hover Download as a Function of Thrust Coefficient

Further insight can be gained regarding tiltrotor download-to-thrust ratio trends by examining the wing sectional download spanwise distribution. Integrated wing pressure data in Fig. 12 allows two observations to be made. First, most of the wing download is generated near the wing tip (close to the rotor axis). Second, as rotor thrust is decreased, proportionally more and more of the wing download is carried at the wing tip. This is a consequence of highly twisted tiltrotor blades only carrying positive thrust on the inboard blade sections (and, thereby, producing a downwash) while the outboard blade is unloaded or negatively-loaded (resulting in very little downwash or, perhaps, even an upwash) at low rotor collectives.
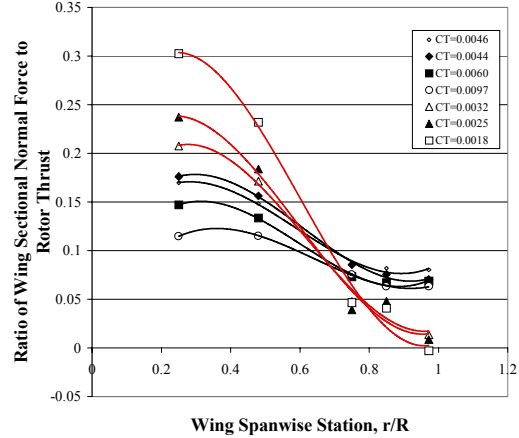

Fig. 12– Wing Sectional Download Distribution as a Function of Rotor Thrust Coefficient

Another qualitative comparison can be made between the full-span TRAM integrated wing pressure hover download data and the Ref. 6 0.658-scale JVX data. Figure 13 shows the dependence of tiltrotor hover download on wing flaperon angle. The qualitative agreement between the Ref. 6 data and the full-span TRAM results is quite good. A flaperon angle of $\delta_f \sim 70$ deg. results in a minimum wing download, for both cases.
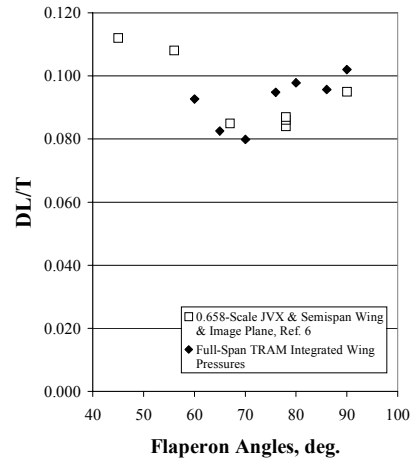

Fig. 13 – Tiltrotor Download as a Function of Flaperon Angles

Insight into the Fig. 13 results can be arrived by considering the wing sectional normal-force-to-thrust ratio spanwise distributions for several flaperon angles, Fig. 14, and selected wing chordwise pressure profiles, Fig. 15a-b. The general character of the spanwise distributions in Fig. 14 does not to appear to change with flaperon angle other than a shift in overall magnitude of the sectional normal-force-to-thrust ratio curves. (The two fitted curves (at δ_f=70 and δ_f=90 deg.) highlight the minimum and maximum observed download measurements.)
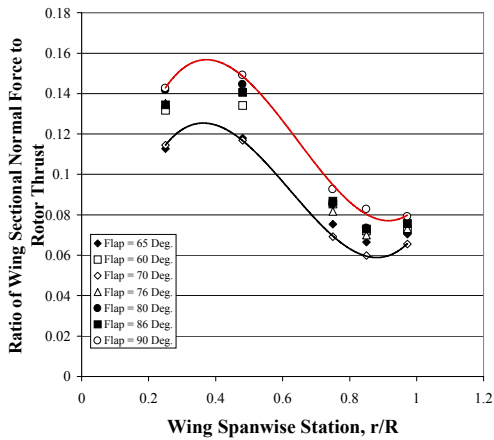
Fig. 14—Wing Download Distribution as a Function of Wing Flaperon Angle (CT=0.008)

The wing chordwise pressure distributions of Fig. 15a-b, for flaperon angles of 60 and 70 degrees (at spanwise stations 0.25 and 0.85 r/R), reveal subtle upper surface pressure profile differences, particularly at the leading and trailing edge of the wing. The lower surface chordwise pressures are indistinguishable from each other.

Chordwise Station (Undeflected Coordinates), x/c
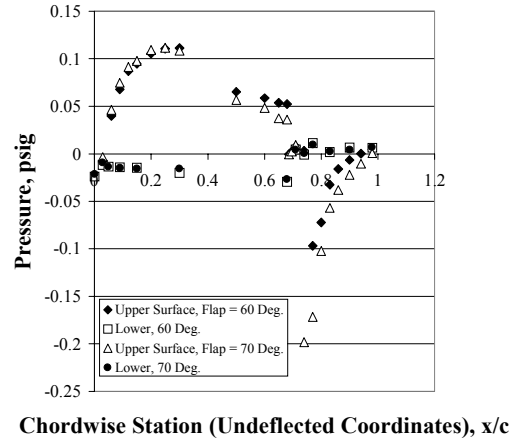
(a) r/R = 0.25
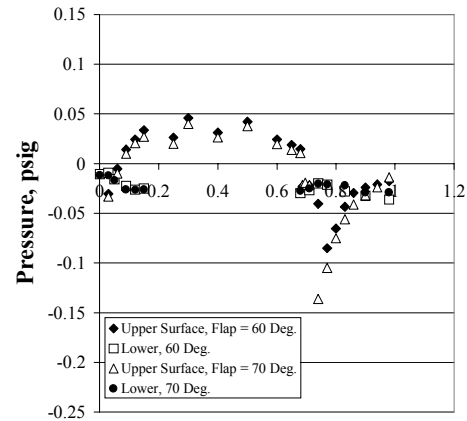
Chordwise Station (Undeflected Coordinates), x/c

(b) r/R = 0.85

Fig 15 – Wing Chordwise Pressure Profiles for Different Flaperon Angles

The full-span TRAM hover download trends are consistent with results obtained with tiltrotor semispan wing and image plane test models, such as Refs. 5 and 6. It is interesting to note that for wing download studies, tiltrotor models using semispan wings and image planes may be sufficient for hover wing download studies. This has been a point of considerable debate within the tiltrotor research community for several years. The same can not necessarily be said for rotor performance measurements; the literature does not reveal anywhere near the level of wing-on-rotor and/or rotor-on-rotor (or image-plane on rotor) interactions on rotor performance for semispan test models as has been observed for the full-span TRAM hover results (Fig. 7).

Rotor and Wing Interactions in Helicopter-Mode Forward-Flight

Figure 16 shows the influence of the wing and airframe (and the second rotor) on rotor performance in helicopter-mode forward flight. The rotor thrust is directly measured from the TRAM rotor balances. The rotor thrust and power coefficient data is shown for an advance ratio, μ, of 0.15. The isolated rotor performance data is from the TRAM DNW test, Ref. 3. Figure 16 can only be considered a preliminary examination of the influence of wing and/or airframe interactions on helicopter-mode forward flight rotor performance. No wind tunnel wall corrections have been applied to the data shown in Fig. 16. As noted in Ref. 8, wind tunnel corrections can be very important for correlating data between tests and between experiment and analysis. In particular, Ref. 8 identified satisfactory corrections for the isolated rotor TRAM DNW data.
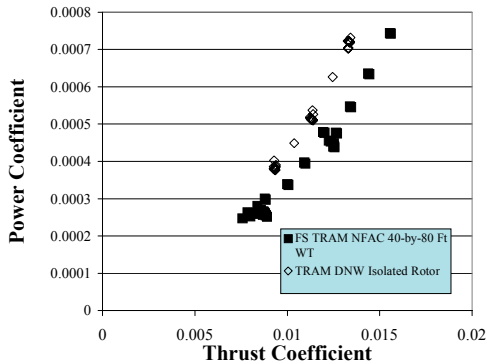

Fig. 16 -- Wing/Airframe on Rotor Interactions in Helicopter Mode Forward Flight ($M_{Tip} = 0.63$, μ=0.15, $\alpha_F = +11$ deg., and $\alpha_S = +6$ deg.)

Hub weight and aerodynamic tares have been applied in Fig. 16 to the rotor power and thrust coefficients for both the isolated rotor and full-span TRAM data sets. In both cases the same methodology (and hub configuration) was used to derive and apply the hub tares. Figure 17 shows the hub tare configurations for the isolated rotor and full-span configurations.

(a) isolated rotor
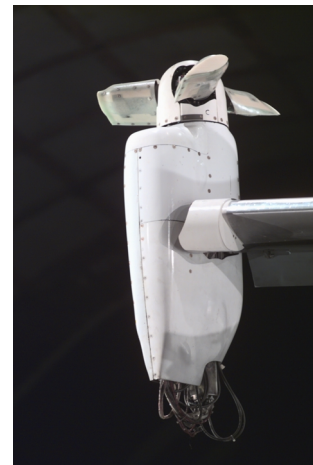
(b) full-span TRAM

Fig. 17 – Hub Tare Configurations

The influence of the rotor wakes on tiltrotor airframe aerodynamics can be seen in Fig. 18 for $\delta_f = 43$ deg., $\delta_e = 0$ deg., and $i_N = 85$ deg. (nacelles pitched five degrees forward of vertical when the fuselage angle of attack is zero degrees). The tunnel velocity is 62 knots. The rotor thrust coefficient for the rotor-on configuration is C_T=0.008. Due to problems with the left hand rotor balance during the helicopter-mode forward flight testing, symmetry has been assumed between the loads for the left and right hand rotor balances and so (two-times) the right hand balance thrust results were subtracted from the fuselage balance loads. The wing is 'clean' – no vortex generators or fences are installed; no forebody strake is represented on the model.
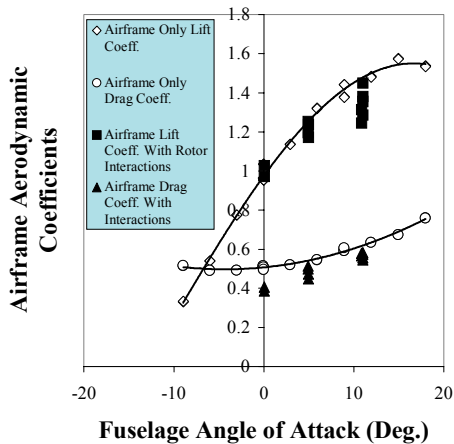
Fig. 18 – Influence of Rotor on Wing/Airframe Interactions on Airframe Lift and Drag

Fig. 20 -- Influence of Rotor Thrust on Tiltrotor Airframe Drag

The rotor-on-wing interactions seen in Fig. 18 are shown further in Figs. 19 and 20. In this case, the influence of varying rotor thrust is even more clearly seen on both the airframe lift and drag results. Figure 19 and 20 are results for a fuselage angle of attack of +11 deg. (and a rotor shaft angle of –5 deg.). Unfortunately, thrust sweeps for other fuselage angles of attack were not acquired during the full-span TRAM test.

Fig. 19 – Influence of Rotor Thrust on Tiltrotor Airframe Lift

Figure 21 shows the influence of rotor-on-wing interactions on wing normal force coefficients, as a function of fuselage angle of attack, as derived from integrated wing pressures. Figure 21 results are for the same model configuration and test conditions as Fig. 18 results – i.e. $C_T=0.008$, $\delta_f = 43$ deg., $\delta_e = 0$ deg., $i_N = 85$ deg, and $\mu=0.15$. The rotor and fuselage balance measurements (Fig. 18) and the integrated wing pressure data (Fig. 21) are both in general agreement as to the effect of rotor-on-wing interactions observed during helicopter-mode forward-flight testing of the full-span TRAM. It appears that the observed effect of the rotor-on-wing interactions is primarily one of influencing the onset and severity of wing stall. This must stem from the rotor wake's unsteady flow adversely interacting with the wing aerodynamics. On the other hand, the mean induced vertical velocities of the rotor wake (at a $C_T=0.008$) do not appear to be of sufficient magnitude to significantly reduce the wing angle-of-attack. More wind tunnel testing will be required to fully understand wing-on-rotor interactions.
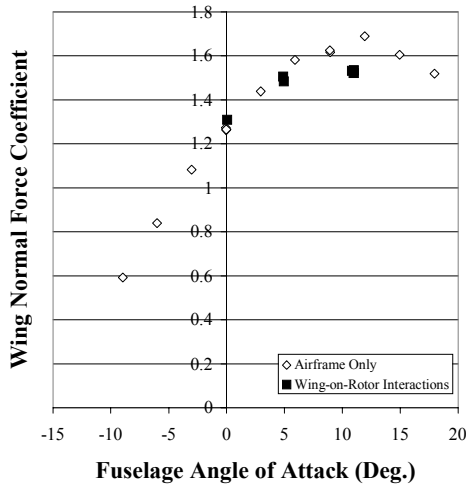
10

Fig. 21 – Effect of Rotor-on-Wing Interactions
on Wing Normal Force Coefficients

Aerodynamics of Airplane-Mode Forward-Flight

Figure 22 shows the TRAM model in its airplane-mode (rotor-off) forward flight configuration. The TRAM model was tested up to 291 knots in this configuration. Fuselage balance and wing pressure data was acquired.

Fig. 22 – Full-Span TRAM in Airplane-Mode
(Rotors Off)

Figures 23 and 24 show the lift curve and lift-drag polars for the full-span TRAM in airplane-mode forward flight. Lift and drag data are presented for two different wing Reynolds numbers: 3.3×10^6 (V = 150 knots) and 6.4×10^6 (V = 291 knots). The airplane-mode

configuration is δ_f = 0 deg., δ_e = –17 deg., and i_N = 0 deg. (δ_e = –17 deg. was primarily set to minimize the pitching moment load carried on the fuselage balance). The lift curve results for Fig. 23 compare reasonably well with Ref. 11 computational and measured results for the V-22 tiltrotor aircraft.
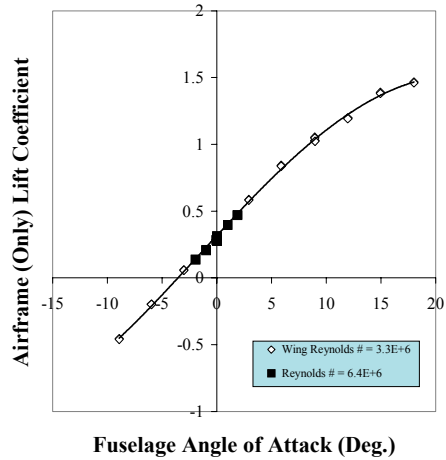

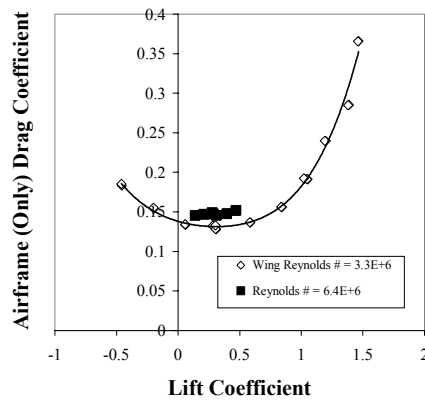Fig. 23 – TRAM Airframe-Only Airplane-Mode
Lift Curves

Fig. 24 – TRAM Airframe-Only Airplane-Mode
Lift/Drag Polar

Tare and interference (T&I) corrections for the model mounting strut have not been made in the lift and drag data presented in Figs. 23 and 24. Attempting to acquire T&I corrections in the 40-by-80 Foot Wind Tunnel with the full-span TRAM installation would be an arduous task that may or may not be feasible given the large size of the facility and test model. As such this

airframe lift and drag data derived from the model fuselage balance can not be fully considered representative of the 'free air' aerodynamics of a tiltrotor aircraft.

Figure 25 are representative wing chordwise pressure distributions for the TRAM wing in airplane-mode forward-flight (rotors-off) for r/R = 0.25 and 0.85, respectively. The fuselage angle of attack is zero degrees and $\delta_f = \delta_e = 0$ deg. The tunnel dynamic pressure is 13.5 psf (tunnel velocity is 63 knots).
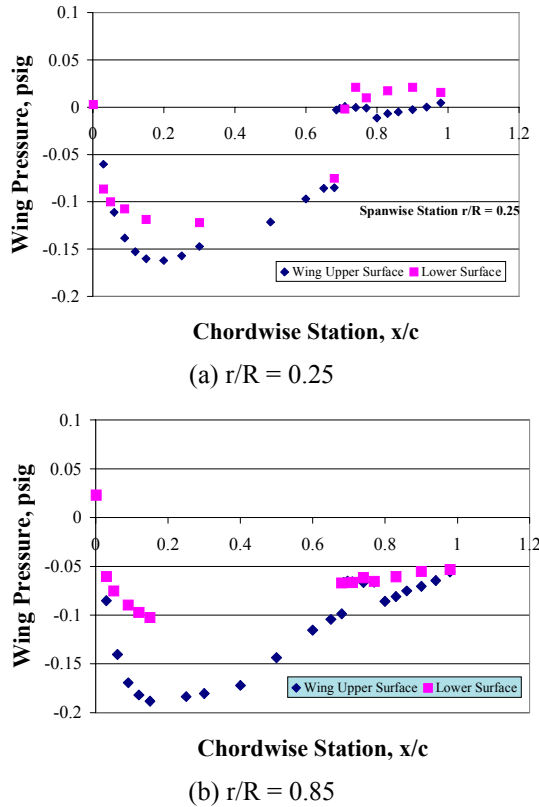
(a) r/R = 0.25

(b) r/R = 0.85

Fig. 25a-b – Representative Airplane-Mode Forward-Flight (Rotors-Off) Wing Pressure Distributions

Tunnel velocity and fuselage angle-of-attack sweeps were performed for the rotor-off airplane-mode testing. Integrated sectional normal force coefficient spanwise distribution estimates can be made from the wing pressure data. Figure 26 shows the (left-hand wing)

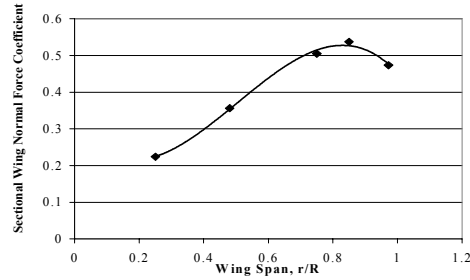normal force coefficient distribution for the same test condition as the Fig. 25 data.

Fig. 26 – Representative Sectional Normal Force Coefficient Spanwise Distribution

The relative contribution of the wing versus the airframe (wing plus fuselage) normal force coefficient can be seen in Fig. 27. The two curves of Fig. 27 were derived from fuselage balance measurements for the airframe normal force coefficient curve and integrated wing pressure data for the wing normal force curve. Two observations can be made from Fig. 27. First, integration of the wing pressure data appears to yield satisfactory integrated aerodynamic coefficients. Second, the fuselage does appear to be a significant contributor to the airframe normal force for large fuselage angles of attack. Future work can focus on comparing full-span TRAM wing pressure data and sectional normal force coefficient properties with existing airfoil, wing, and unpowered force model for the V-22 tiltrotor aircraft (Refs. 11 and 12, for example).
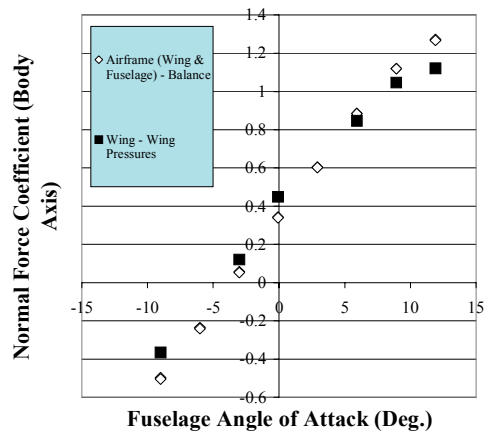

Fig. 27 – Airframe Versus Wing Normal Force Coefficient Contribution ($i_N = 0$ deg., $\delta_f = 0$ deg., $\delta_e = -17$ deg., V = 104 knots, Re = 2.3×10^6)

The wing sectional normal force coefficient spanwise distributions for the Fig. 27 data are shown in Fig. 28. Figure 28 is based on integrated wing pressure data. Over all, given the results of Figs. 27 and 28, reasonable wing sectional normal force values can be derived form the full-span TRAM wing pressure data. This data will be a valuable aid in the refinement of comprehensive rotorcraft aeromechanics analysis tools and computational fluid dynamics analyses.
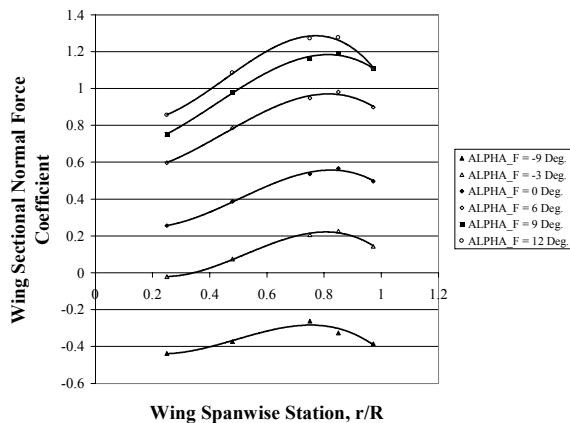

Fig. 28 – Influence of Fuselage Angle of Attack on Wing Spanwise Distributions

Concluding Remarks

The paper discusses in detail several observed tiltrotor aerodynamic characteristics as evidenced by the TRAM wing static pressure and model balance load measurements. These airframe aerodynamics and rotor and wing interaction observations encompass three primary operating regimes for tiltrotor aircraft: hover, helicopter-mode forward flight, and airplane-mode cruise forward flight. Comparisons are made between isolated rotor TRAM data acquired in the DNW wind tunnel and data from the recent full-span TRAM test in the Ames Research Center NFAC 40-by-80 Foot Wind Tunnel. Hover results are compared between the 0.25-scale full-span TRAM and previously reported 0.658-scale JVX proprotor and semispan wing tests results acquired in the NFAC. The results from this paper, though preliminary in nature, point to several important

interactional aerodynamic phenomena for tiltrotor aircraft.

The Tilt Rotor Aeroacoustic Model project continues to explore fundamental tiltrotor aeromechanics and aeroacoustics. Planning for follow-on tests are currently underway. This major research investment on the part of NASA and the U.S. Army will enable the development of a new generation of tiltrotor analytical design tools and advanced tiltrotor technologies.

Acknowledgements

References

1. Young, L. A., "Tilt Rotor Aeroacoustic Model (TRAM): A New Rotorcraft Research Facility," American Helicopter Society (AHS) International Specialist's

Meeting on Advanced Rotorcraft Technology and Disaster Relief, Gifu, Japan, April 1998.

2. Johnson, J.L. and Young, L.A., "Tilt Rotor Aeroacoustic Model Project," Confederation of European Aerospace Societies (CEAS) Forum on Aeroacoustics of Rotors and Propellers, Rome, Italy, June 9-11, 1999.

3. Young, L. A., Booth, E. R., Yamauchi, G. K., Botha, G., Dawson, S., "Overview of the Testing of a Small-Scale Proprotor," 55th Annual Forum of the American Helicopter Society, Montreal, Canada, May 25-27, 1999.

4. McCluer, M.S. and Johnson, J.L., "Full-Span Tiltrotor Aeroacoustic Model (FS TRAM) Overview and Initial Testing," American Helicopter Society Aerodynamics, Acoustics, and Test and Evaluation Specialist Meeting, San Francisco, CA, January 23-25, 2002.

5. Felker, F,F. Signor, D, Young, L.A., and Betzina, M., "Performance and Loads Data From a Hover Test of a 0.658-Scale V-22 Rotor and Wing," NASA TM 89419, April 1987.

6. Felker, F.F., Shinoda, P.R., Heffernan, R.M., and Sheehy, H.F., "Wing Force and Surface Pressure Data form a Hover Test of a 0.658-Scale V-22 Rotor and Wing," NASA TM 102244, February 1990.

7. McVeigh, M.A., Grauer, W.K., and Paisley, D.J., "Rotor/Airframe Interactions on Tiltrotor Aircraft," Journal of the American Helicopter Society, Vol. 35 – No. 3, July 1990.

8. Johnson, W., "Calculation of Tilt Rotor Aeroacoustic Model (TRAM DNW) Performance, Airloads, and Structural Loads," American Helicopter Society Aeromechanics Specialist Meeting, Atlanta, Georgia, November 13-15, 2000

9. Liu, J., McVeigh, M.A., Mayer, R.J., and Snider, R.W., "Model and Full-Scale Tiltrotor Hover Download Tests," 55th Annual Forum of the American Helicopter

Society, Montreal, Quebec, Canada, May 25-27, 1999.

10. Wood, T.L. and Peryea, M.A., "Reduction of Tiltrotor Download," 49th Annual Forum of the American Helicopter Society, St. Louis, Missouri, May 19-21, 1993.

11. Carlin, G.J., Staedeli, W.E., and Hodges, R.M., "Analysis of V-22 Tilt-Rotor Aircraft Using Panel Methods," 42nd Annual Forum of the American Helicopter Society, Washington, DC, June 1986.

12. Narramore, J.C., "Airfoil Design, Test, and Evaluation for the V-22 Tilt Rotor Vehicle," 43rd Annual Forum of the American Helicopter Society, St. Louis, Missouri, May 18-20, 1987.